Video Article

Quantification of Strain in a Porcine Model of Skin Expansion Using Multi-View Stereo and Isogeometric Kinematics

Adrian Buganza Tepole[1], Elbert E. Vaca[2], Chad A. Purnell[2], Michael Gart[2], Jennifer McGrath[2], Ellen Kuhl[3], Arun K. Gosain[2]

[1]Mechanical Engineering, Purdue University

[2]Division of Plastic Surgery, Ann and Robert H. Lurie Children's Hospital of Chicago, Northwestern University Feinberg School of Medicine

[3]Mechanical Engineering, Bioengineering, Cardiothoracic Surgery, Stanford University

Correspondence to: Adrian Buganza Tepole at abuganza@alumni.stanford.edu

URL: https://www.jove.com/video/55052
DOI: doi:10.3791/55052

Keywords: Bioengineering, Issue 122, Skin, Tissue expansion, Multi-view stereo, Isogeometric analysis, Porcine model, Spline

Date Published: 4/16/2017

Citation: Buganza Tepole, A., Vaca, E.E., Purnell, C.A., Gart, M., McGrath, J., Kuhl, E., Gosain, A.K. Quantification of Strain in a Porcine Model of Skin Expansion Using Multi-View Stereo and Isogeometric Kinematics. *J. Vis. Exp.* (122), e55052, doi:10.3791/55052 (2017).

Abstract

Tissue expansion is a popular technique in plastic and reconstructive surgery that grows skin *in vivo* for correction of large defects such as burns and giant congenital nevi. Despite its widespread use, planning and executing an expansion protocol is challenging due to the difficulty in measuring the deformation imposed at each inflation step and over the length of the procedure. Quantifying the deformation fields is crucial, as the distribution of stretch over time determines the rate and amount of skin grown at the end of the treatment. In this manuscript, we present a method to study tissue expansion in order to gain quantitative knowledge of the deformations induced during an expansion process. This experimental protocol incorporates multi-view stereo and isogeometric kinematic analysis in a porcine model of tissue expansion. Multi-view stereo allows three-dimensional geometric reconstruction from uncalibrated sequences of images. The isogeometric kinematic analysis uses splines to describe the regional deformations between smooth surfaces with few mesh points. Our protocol has the potential to bridge the gap between basic scientific inquiry regarding the mechanics of skin expansion and the clinical setting. Eventually, we expect that the knowledge gained with our methodology will enable treatment planning using computational simulations of skin deformation in a personalized manner.

Video Link

The video component of this article can be found at https://www.jove.com/video/55052/

Introduction

Tissue expansion is a common technique in plastic and reconstructive surgery that grows skin *in vivo* for the correction of large cutaneous defects [1]. Neumann, in 1957, was the first surgeon to document this procedure. He implanted a balloon below the skin of a patient and inflated it gradually over a period of several weeks to grow new tissue and resurface an ear [2]. Skin, like most biological tissues, adapts to applied forces and deformations in order to reach mechanical homeostasis. When stretched beyond the physiological regime, skin grows [3,4]. One of the central advantages of tissue expansion is the production of skin with proper vascularization and the same hair bearing, mechanical properties, color, and texture as the surrounding tissue [5].

After its introduction six decades ago, skin expansion has been widely adopted by plastic and reconstructive surgeons and is presently used to correct burns, large congenital defects, and for breast reconstruction after mastectomy [6,7]. Yet, despite its widespread use, skin expansion procedures can lead to complications [8]. This is partly due to the lack of sufficient quantitative evidence needed to understand the fundamental mechanobiology of the procedure and to guide the surgeon during preoperative planning [9,10]. Key parameters in this technique are the filling rate, filling volume per inflation, the selection of the shape and size of the expander, and the placement of the device [11,12]. Current preoperative planning relies largely on the physician's experience, resulting in a wide variety of arbitrary protocols that often differ greatly [13,14,15].

To address the current knowledge gaps, we present an experimental protocol to quantify expansion-induced deformation in a porcine animal model of tissue expansion. The protocol relies on the use of multi-view stereo (MVS) to reconstruct three-dimensional (3D) geometries out of sequences of two-dimensional (2D) images with unknown camera positions. Employing splines, representation of smooth surfaces leads to the calculation of the corresponding deformation maps by means of an isogeometric (IGA) description. The analysis of the geometry is based on the theoretical framework of continuum mechanics of membranes having an explicit parameterization [16].

Characterizing physiologically relevant deformations of living materials over long periods of time still remains a challenging problem. Common strategies for imaging of biological tissues include stereoscopic digital image correlation, commercial motion capture systems with reflective markers, and biplane video fluoroscopy [17,18,19]. However, these techniques require a restrictive experimental setup, are generally expensive, and have been primarily used for *ex vivo* or acute *in vivo* settings. Skin has the advantage of being a thin structure. Even though it consists of several layers, the dermis is largely responsible for the mechanical properties of the tissue and thus the surface deformation is of primary importance [20]; reasonable kinematical assumptions can be made regarding the out of plane deformation [21,22]. Moreover, skin is already exposed to the outside environment, making it possible to use conventional imaging tools to capture its geometry. Here we propose the use of MVS as an affordable and

flexible approach to monitor *in vivo* deformations of skin over several weeks without interfering majorly with a tissue expansion protocol. MVS is a technique that extracts 3D representations of objects or scenes from a collection of 2D images with unknown camera angles [23]. Only in the last three years, several commercial codes have appeared (see list of materials for examples). The high accuracy of the model reconstruction with MVS, with errors as low as 2% [24], makes this approach suitable for the kinematic characterization of skin *in vivo* over long periods of time.

To obtain the corresponding deformation maps of skin during tissue expansion, points between any two geometric configurations are matched. Conventionally, researchers in computational biomechanics have used finite element meshes and inverse analysis to retrieve the deformation map [25,26]. The IGA approach employed here uses spline basis functions which offer several advantages for the analysis of thin membranes [27,28]. Namely, the availability of high degree polynomials facilitates representations of smooth geometries even with very coarse meshes [29,30]. Additionally, it is possible to fit the same underlying parameterization to all the surface patches, which circumvents the need for an inverse problem to account for non-matching discretizations.

The method described here opens new avenues to study skin mechanics in relevant *in vivo* settings over long periods of time. In addition, we are hopeful that our methodology is an enabling step towards the ultimate goal of developing computational tools for personalized treatment planning in the clinical setting.

Protocol

This protocol involves animal experiments. The protocol was approved by the IRB of Ann and Robert H. Lurie Children's Hospital of Chicago Research Center Animal Care and Use Committee to guarantee humane treatment of animals. The results for two expansion studies using this protocol have been published elsewhere [16,31].

Execution of this protocol requires a team with complementary expertise. The first part of the protocol describes the surgical procedure on the animal model, requiring personnel with the appropriate medical training. The subsequent analysis, particularly sections 4 and 5, involve basic computer programming skills in C++ and Python, and use of a command line shell.

1. Surgical Procedure for Expander Placement

NOTE: Personnel involved in the operation must be scrubbed and gowned in a sterile fashion. Sterile towels and drapes are applied around the surgical field to maintain sterility. All instruments, sutures, and tissue expanders are received in sterile packaging and handled only by sterile personnel. Sterility of the operative site must not be violated until the procedure is complete.

1. Acclimate one-month-old male Yucatan mini pigs to standard housing for one week, and feed *ad libitum*.
2. On the day of surgery, anesthetize the animal using ketamine/acepromazine for induction (4 - 6 mg/kg), then isoflurane for maintenance. Evaluate depth of anesthesia by monitoring the palpebral reflex. Also, monitor vital signs (heart rate, body temperature, respiratory rate, and/or response to pinch by tissue forceps). Apply ophthalmic ointment to the eyes to protect against corneal abrasions.
3. Administer pre-procedural antibiotics and clean the dorsal skin with chlorhexidine-based surgical soap. Transfer four 10 x 10 cm^2 grids, two on each side of the animal, with 1 cm line markings to the pig skin using tattoo transfer medium. The grids correspond to the following four regions: left rostral, right rostral, left caudal, and right caudal. Use a template with a midline reference to ensure symmetric placement of the grid patterns.
    1. Create the grids on paper by tracing the grid outlines heavily with a ballpoint pen. Wash the area on the animal where the grid is to be placed with isopropyl rubbing alcohol.
    2. Apply the grid (pen-ink side down) directly onto the skin. The alcohol serves to *leech* some of the ink off of the paper, transferring the grid to the animal's skin.
4. Inject local anesthetic (1% lidocaine with 1:100,000 epinephrine) subcutaneously at the site of each planned incision.
5. Make an incision on either side of the animal in the midpoint between the two grids.
   NOTE: The incisions are placed on the left and right side of the animal between the 2 grids on that side. There is a left sided incision and a right sided incision
6. Use a hemostat to develop a subcutaneous tunnel beneath the grid of interest. After developing a tunnel, insert the expander beneath the grid.
   NOTE: Tunnels are placed under any grid that will have a tissue expander.
7. Place the port for expander inflation remotely through a subcutaneous tunnel developed in a similar fashion along the dorsal midline of the animal. Repair wounds by suturing.
8. Postoperatively, treat the animal with prophylactic antibiotics (Ceftiofur 5 mg/kg IM once) as well as analgesics (Buprenorphine 0.05 - 0.1 mg/kg) via intramuscular injection every 12 h for 4 doses, with additional doses available for evidence of animal distress.
9. Observe animals continuously for 2 h postoperatively, including routine measurement of vital signs until they have resumed ambulation and are able to maintain normothermia. House the animal in a separate cage and monitor until it is able to walk independently on all 4 legs before transferring it back to its normal housing area and leaving it unattended.
10. Following the immediate post anesthesia recovery period, check animals daily to evaluate wound healing. Remove the sutures 14 days postoperatively. These incisions do not require dressings. Leave the incisions to heal for 3 - 4 weeks before beginning expansion

2. Inflation Protocol

NOTE: The timing of the inflations and amount of solution used in each expander depends on the specific question being studied. To characterize the effect of different expander geometries, a suitable protocol is to perform five inflation steps at 0, 2, 7, 10, and 15 days to achieve filling volumes of 50, 75, 105, 165, and 225 cc respectively.

1. Before each inflation step, sedate the animal administering ketamine (4 - 6 mg/kg) and dexmedetomidine at 20 - 80 µg/kg.

NOTE: Dexmedetomidine is an alpha-adrenergic agonist that can be reversed with atipamezole (1:1 volume:volume) to facilitate faster recovery; however, this level of sedation may not be adequate for the animal to tolerate expansion without undue risk of harm to the animal or handlers. If this is the case, administer general anesthesia by delivering isoflurane via mask ventilation following ketamine/acepromazine induction.

2. Attach two plastic flexible tape measures to the skin of the animal using surgical tape. Place the tape measures between the grids on the left and right sides.
3. Place the animal on one side and acquire 30 photographs of the scene from as many different angles as possible.
   NOTE: The objective is to capture the geometry of the two grids visible when the animal is laying down on one side.
   1. First, position the camera above the animal and leaning towards the caudal side, to capture a shot where the tattooed grids are fully visible and fill the frame.
   2. Move in a circular pattern around the animal in an arch from the caudal to the rostral direction, taking photographs along the way, ensuring that, for every photograph, the tattooed grids that are visible appear entirely in the frame.
      1. At the same time, try to maximize the space that the grids occupy in the frame. An ideal shot would capture the back of the animal with the tattooed grids and only small regions of background.
   3. Next, position the camera towards the ventral side to capture a shot angle that is approximately parallel to the ground and take photographs in an arch from the ventral to the dorsal region.
      NOTE: The amount of photographs is not a fixed value. For a good reconstruction, every point on the tattooed grid should be in at least 3 photographs; 30 photographs in total is an adequate amount for successful geometry reconstruction.
4. Place the animal on the opposite side and take 30 photographs of the two remaining grids following the same steps outlined above.
5. Perform the inflation step by finding the remote filling port and injecting the required amount of saline solution corresponding to the expansion protocol of interest. Use sterile 0.9% injectable saline.
   1. Locate the ports and prep over the skin of the animal with isopropyl alcohol wipes. Access the port with a sterile 25-gauge butterfly needle attached to a syringe filled with sterile injectable saline.
      NOTE: As described above, the ports are tunneled subcutaneously to a position on the anterior midline dorsum during expander placement.
   2. Inject the desired amount of saline solution. Please refer to the note at the beginning of this section for the inflation volumes injected at each step of the expansion process.
6. Repeat the photo acquisition steps after inflation.
7. Once the inflation protocol is complete, euthanize the animals.
   1. Administer general anesthesia by delivering isoflurane via mask ventilation following ketamine/acepromazine induction. Evaluate depth of anesthesia by monitoring the palpebral reflex. Also, monitor vital signs (heart rate, body temperature, respiratory rate, and/or response to pinch with tissue forceps).
   2. Euthanize the animal by intravenous overdose of pentobarbital 90 - 100 mg/kg. Following pentobarbital overdose for euthanasia, confirm death by the absence of detectable heartbeat using a pulse oximeter and pulse palpation as well as the absence of spontaneous respirations.

3. Multi-view Stereo Reconstruction

1. Use commercially available software to upload the image files and reconstruct the geometric models.
   1. Launch the MVS software on the browser and log in.
   2. Select ***Photo to 3D*** on the top left corner.
   3. Click ***add photos***, browse to the location of the images and manually select the 30 photographs corresponding to a single model.
   4. Name the model and click *create*
   5. Wait for the model to be created. This can take several minutes. Click ***dashboard*** on the right to go back to the original landing page of the software.
      NOTE: The dashboard shows representative images of the geometric models that have been created by the user.
   6. Place the cursor on the model that has just been created. Place the cursor on the bottom right corner of the model image. Click ***downloads*** and select ***obj***.

4. Spline Surface Fit

1. Use open source software to process the geometric models.
2. Click ***File->Import->obj*** to import the file generated from the MVS software. On the bottom of the 3D View click on ***Viewport Shading*** and select ***Texture***. Look for a tab on the right of the 3D View with the submenus: ***Transform***, ***Grease Pencil***, ***View***, ***3D Pencil***, *etc.* Click on ***Shading*** and select ***Shadeless***.
3. Right click on the geometry to select it. On the bottom of the 3D View select ***Edit Mode*** to visualize the triangular mesh.
4. Select one by one the nodes on the 1 cm markings of the tape measure.
   1. To select a point, right click on it, and highlight the point. Coordinates for the point appear on the tab on the right-hand side of the 3D View. Select and copy the coordinates of the selected point to a text file.
   2. Repeat this operation for all the points on the 1 cm markings of the tape measure.
   3. Do this for both tape measures. Examples of coordinate text files are provided: *tape1.txt, tape2.txt*.
      NOTE: If there are no nodes of the mesh on the point of interest, subdivide the mesh until there is a node on the point of interest. To subdivide the mesh select the three vertices of a triangle by pressing *Shift* key and right-clicking on the vertices. Then click on the

button *Subdivide* on the tab appearing on the left-hand side of the 3D View. This operation adds three more nodes inside the selected triangle.

5. Select the 11 x 11 points of the grid and save the coordinates of the 121 points to a text file in the pattern shown in **Figure 1**.
    1. Analogously to what was done for the tape measures, to select a point of the grid, right click on it, the point will be highlighted. Coordinates for the point will appear on the tab on the right-hand side of the 3D View. Select and copy the coordinates of the selected point to a text file
    NOTE: The numbering of the grid points is always caudal to rostral and from the dorsal midline towards the ventral region. This ordering guarantees that the parameter space is consistent for any two patches. As an example, the file *gridReference.txt* which contains the coordinates of 121 points of a skin patch is provided.

6. Download, compile and install C++ spline libraries. The file *splineLibraryInstallation.txt* contains the link to the source code of the spline libraries and instructions for installation.
7. Compile the source code *generateCurve.cpp* to generate the executable *generateCurve*
NOTE: The program *generateCurve* only needs to be compiled once. To compile this C++ source code and generate an executable follow the instructions at the top of the source code file *generateCurve.cpp.*
8. Use the program *generateCurve* to fit splines to the tape measures and to the grid points. To run the executable in a Bash shell, type
directory$ ./generateCurve
    1. Upon running the program, it will ask the user to type in the path to the file containing the coordinates of the tape measure. Then the program will ask for a name for the output file. Add the termination *.g2* to the filename.
    NOTE: The termination *.g2* stands for *go tools*, and is associated to the spline libraries. Two examples of spline files corresponding to the tape measures are available with this protocol (*tape1.g2, tape2.g2*).

9. Use the Python script *scalePoints.py* to scale the grid points. Run the program in a Bash shell prompt with three arguments: the filename of the grid points and the file names of the splines corresponding to the tape measures
directory$ python scalePoints.py gridReference.txt tape1.g2 tape2.g2
NOTE: The script *scalePoints.py* imports the scripts *B_spline.py* and *NURBS_Curve.py*, therefore all three scripts must be in the same folder.
10. Compile the source code *generateSurface.cpp* to generate the executable *generateSurface*.
NOTE: This step only needs to be done once. More detailed instructions are available at the beginning of the source code file *generateSurface.cpp*.
11. Use the program *generateSurface* to fit a spline surface to the grid points. Run the executable *generateSurface* on the Bash shell
directory$ ./generateSurface
    1. Running the program in a shell will ask for the filename containing the scaled points. Then it will ask for the name of the output file. Add the termination *.g2* to the output filename.
    NOTE: The termination *.g2* is suggested by the spline libraries and stands for *go tools*. The files *gridReference.g2* and *gridDeformed.g2* are provided as examples.

5. Quantification of Expansion-induced Deformation

1. Start Python in the Bash shell prompt
directory$ python
NOTE: Python initializes the *interpreter,* which is an interface similar to the shell that will show a new command line environment >>>
2. Import the script *expansionIGA.py* which contains a function called *evaluateMembraneIGA*
>>> from expansionIGA import evaluateMembraneIGA
3. Call the function *evaluateMembraneIGA* to calculate the deformation maps.
NOTE: This function takes as arguments:
Filename of the reference surface
Filename of the deformed surface
Resolution of the evaluation (how many points are evaluated in each direction)
Minimum value of area stretch used to scale the contour plot
Maximum value of area stretch used to scale the contour plot
Minimum value of stretch in longitudinal direction used to scale the contours
Maximum value of stretch in longitudinal direction used to scale the contours
Minimum value of stretch in transverse direction used to scale the contours
Maximum value of stretch in transverse direction used to scale the contours
Spacing between grid lines in the contour plot
Output filename
    1. For example, run
    >>> evaluateMembraneIGA('gridReference.g2', 'gridDeformed.g2', 250, 3, 0.5, 2, 0.5, 2, 0.5, 25, 'deformation')
    NOTE: This command will generate and save six output files. Note that the last argument in the example above is the output filename *deformation*, thus, the files that will be generated are:
    deformation_theta.png: contour plot of the area stretch
    deformation_theta.txt: table of values corresponding to the contour plot of area stretch
    deformation_G1.png: contour plot of the stretch along the longitudinal axis of the animal
    deformation_G1.txt: table of values corresponding to the contour plot of stretches along the longitudinal axis of the animal
    deformation_G2.png: contour plot of the stretch component in the transverse axis of the animal
    deformation_G2.txt: table of values corresponding to the contour plot of the component of the stretch in the transverse axis of the animal

NOTE: Do not confuse the termination of the spline files, *.g2,* with the vector *G2*. The spline files have ending *.g2* following the naming conventions of the spline library. On the other hand, the vectors *G1* and *G2* denote the longitudinal and transverse directions with respect to the animal.
NOTE: The contour files are generated with distinct features at the four corners to facilitate interpretation of the parameter space: Black pixel: most caudal, most dorsal point; Red pixel corner: most rostral, most dorsal point; Green pixel corner: most caudal, most ventral point; Blue pixel corner: most rostral, most ventral point.

Representative Results

This methodology has been successfully employed to study the deformation induced by different expander geometries: rectangle, sphere and crescent expanders [31,32]. The results corresponding to the sphere and crescent expanders are discussed next. **Figure 2** illustrates the three steps of MVS model reconstruction. The starting point is a collection of photographs from a static scene. The animal with the tattooed grids and the tape measures was lying still as the photographs were taken from different angles. The MVS algorithm matched features between the photographs to extract 3D coordinates. As a result, a geometric model consisting of a triangular mesh with texture was generated.

The protocol described here can be used to investigate different aspects of the tissue expansion process. The variations in regional strains induced by sphere and crescent expanders is one important aspect of the expansion process since it leads to regional variations in the amount of skin grown. Both devices were filled to the same volume at every time point. Five inflation steps were performed at 0, 2, 7, 10, and 15 days to generate filling volumes of 50, 75, 105, 165, and 225 cc. **Figure 3** shows photographs of the expanded skin grids at the end of each inflation step. The expanders stretched the skin and the deformation was apparent by the distortion of the grid over time.

For every configuration of the grid a spline surface was generated as described in the Protocol section. Deformations were calculated by choosing a reference and a deformed grid as illustrated in **Figure 1**. The results of two different types of analyses are discussed here. To study the chronic deformation, the pig at day 0 was selected as the reference configuration and compared to all other time points. Comparing the end of every inflation step to the reference configuration results in the contour plots shown in **Figure 4**. The methodology presented here extracts three measures of deformation. The area change is denoted θ, the stretch in the longitudinal direction is termed λ_{G1}, and λ_{G2} is the stretch in the transverse direction, as shown in **Figure 1**. The progression of the area changes and stretches in the two orthogonal directions for sphere and crescent expanders are depicted in **Figure 4**. Spline surfaces are generally smooth and therefore the corresponding contour plots were smooth. Nonetheless, the coarseness of the mesh was evidenced by the contours which showed spot features. A finer grid would increase the fidelity of the deformation maps. Nevertheless, the differences between different expander geometries was immediately apparent and quantifiable. Even though both expanders were filled to the same volume, the spherical expander induced a larger deformation. The spatial variation of the contour plots revealed that skin was stretched more at the center of the expander compared to the periphery of the grid. Results are summarized in **Table 1**.

A second analysis consisted of determining the acute deformation at every inflation step. In this case, the reference configuration was the grid just prior to expansion, and the deformed grid was that immediately after the inflation step. The deformations induced at every inflation step were remarkably similar on average between the different time points. The summary is contained in **Table 2**. On average, the deformation was close to 1 (where 1 would be the absence of deformation). Inspection of the contour maps shown in **Figure 5** showcased evident spatial variations. Even though there was almost no deformation on average, some zones of the grid were stretched while others were shrunk with respect to the reference. Similar to the analysis of the chronic deformation, the center regions were the ones being stretched the most.

In both the acute and chronic cases, longitudinal and transverse stretches showed a clear trend indicative of anisotropy. Skin, as most collagenous tissues, shows a preferred fiber orientation contributing to an anisotropic mechanical response [25]. In the case of skin in the back of a pig, fibers are thought to be aligned transversely [33]. Our experiments showed that during skin expansion, the stretches in the longitudinal directions were always greater than those along the transverse direction. This was true for both the sphere and the crescent expanders, at all time points, and for the acute and chronic deformation contours. This result supports the hypothesis that skin anisotropy can impact the deformations induced during a tissue expansion procedure.

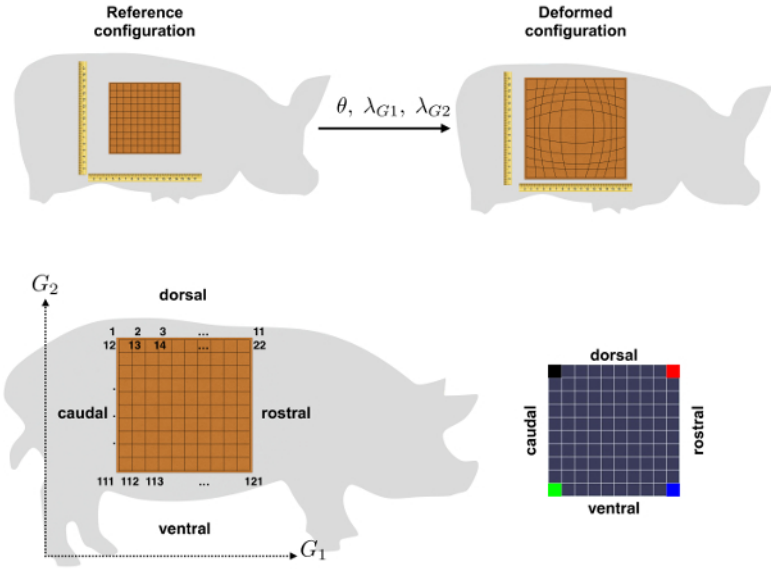

Figure 1: Grid Configurations and Parameter Space. Grids are tattooed on the back of the animals and photographed with tape measures in place in order to scale the geometric models (top). Deformation between a reference and a deformed configuration is characterized by three variables: area change θ, longitudinal stretch λ_{G1}, and transverse stretch λ_{G2} (top). The grid is consistently parameterized by numbering the points always from *caudal* to *rostral* and from *dorsal* to *ventral* directions (bottom left). The output of the analysis is a contour plot over the parameter space. The contours are marked at the corners with one pixel which takes the color black, red, green, and blue, to facilitate identification of *caudal*, *rostral*, *dorsal,* and *ventral* sides (bottom right). Please click here to view a larger version of this figure.

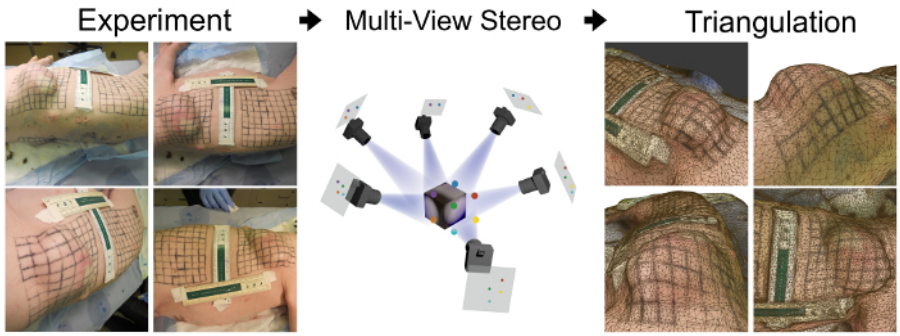

Figure 2: Multi-view Stereo Reconstruction of an Expansion Process. MVS is an algorithm from computer vision that takes as input photographs from different angles with unknown camera positions (left). The algorithm matches features across the images to find 3D coordinates (center). The output of the algorithm is a triangular mesh with the texture overlaid (right). (Figure adapted with permission from [31]) Please click here to view a larger version of this figure.

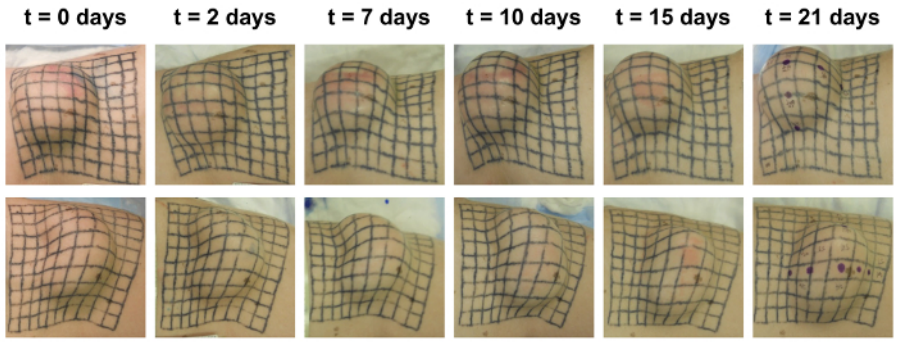

Figure 3: Expansion of Sphere and Crescent Expanders. Sphere (top row) and crescent (bottom row) expanders were placed below the tattooed skin on the back of a pig and inflated at days 0, 2, 7, 10, and 15 days to generate filling volumes of 50, 75, 105, 165, and 225 cc. (Figure adapted with permission from [31]). Please click here to view a larger version of this figure.

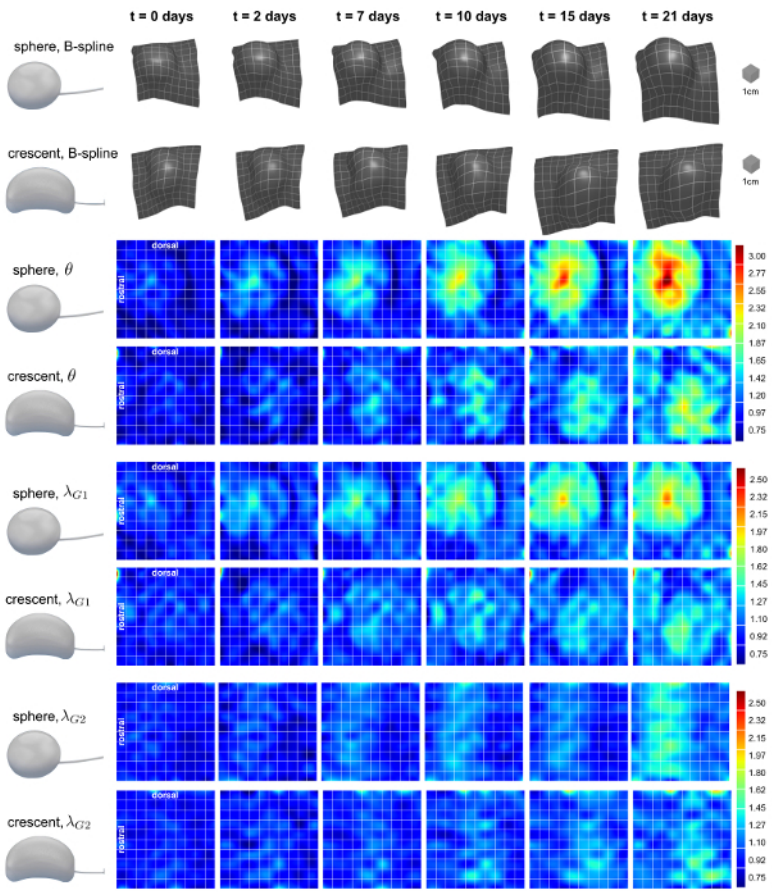

Figure 4: Chronic Deformation Induced by Sphere and Crescent Expanders. The tattooed grids were converted to spline surfaces for analysis (rows 1 and 2). Taking the reference to be the grid at day 0, three measures of deformation were calculated. Area change showed progressively higher values over time, with higher deformation in the center region of the expander, and higher deformation in the sphere compared to the crescent (rows 3 and 4). Longitudinal stretches (rows 5 and 6) resembled area stretches while transverse stretches (rows 7 and 8) showed bands of deformation and less stretch compared to the longitudinal direction. (Figure adapted with permission from [31]) Please click here to view a larger version of this figure.

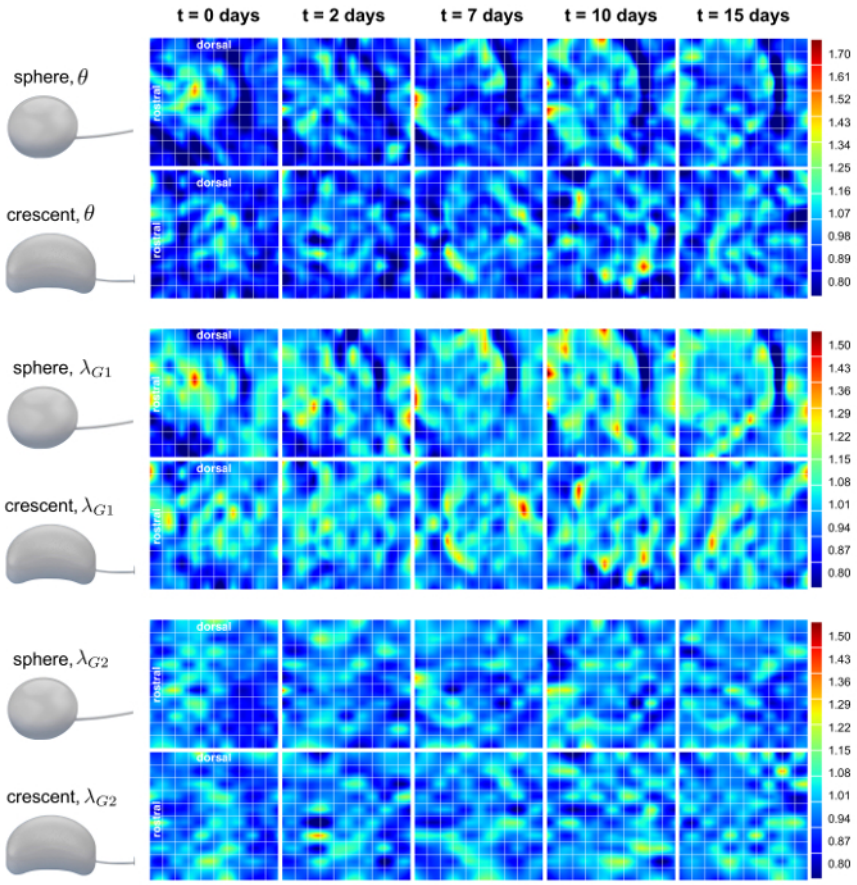

Figure 5: Acute Deformation Induced by Sphere and Crescent Expanders. Taking as reference the configuration just prior to an inflation step, and as deformed the configuration immediately after injection of solution into an expander, acute deformations were calculated. Deformation maps were smooth, however, some edge effects were noticeable and the coarseness of the discretization was reflected in spot-like patterns of deformation. Area changes (rows 1 and 2) showed regional variation, with higher stretch in the region corresponding to the expander. Stretches were similar across the different time points. The same trend could be seen for longitudinal stretches (rows 3 and 4). Transverse stretches (rows 5 and 6) showed more uniform distributions and lower values compared to the longitudinal case. (Figure adapted with permission from [31]) Please click here to view a larger version of this figure.

Time [days]	Expander	Volume [cc]	Area change θ			Longitudinal stretch λ_{G1}			Transverse stretch λ_{G2}		
			max	min	avg	max	min	avg	max	min	avg
0	sphere	50	1.44	0.71	0.98	1.37	0.76	1	1.17	0.84	0.97
0	crescent	50	1.46	0.76	0.98	1.24	0.79	1	1.17	0.84	0.98
2	sphere	75	1.74	0.68	1.08	1.51	0.73	1.08	1.19	0.75	1
2	crescent	75	1.43	0.66	1	1.31	0.65	1	1.26	0.77	1
7	sphere	105	0.01	0.69	1.21	1.7	0.75	1.13	1.32	0.84	1.07
7	crescent	105	1.66	0.83	1.15	1.4	0.87	1.11	1.33	0.86	1.03
10	sphere	165	2.26	0.74	1.36	1.76	0.77	1.21	1.39	0.83	1.11
10	crescent	165	1.86	0.87	1.26	1.58	0.8	1.15	1.45	0.83	1.09
15	sphere	225	2.77	0.72	1.52	2.01	0.69	1.29	1.47	0.89	1.18
15	crescent	225	1.87	0.83	1.32	1.46	0.84	1.17	1.44	0.92	1.14
21	sphere	225	3.09	0.93	1.7	2.13	0.9	1.33	1.62	0.98	1.27
21	crescent	225	2.25	0.87	1.49	1.66	0.85	1.25	1.67	0.96	1.2

Table 1: Summary of Chronic Deformation. Strains were calculated taking the initial configuration as the reference and comparing the patches at the end of each inflation step with respect to it. The average of the deformation attributed to the sphere expander reached 1.70 at day 21 while the crescent expander deformed 1.49 in area by the end of expansion. There was significant spatial variation and maximum and minimum values

varied with respect to the average. The longitudinal stretches reached 1.33 and 1.25 for the sphere and crescent expanders respectively, while transverse stretches were lower, with values of 1.27 and 1.20. (Table adapted with permission from [31])

Time [days]	Expander	Volume [cc]	Area change θ			Longitudinal stretch λ_{G1}			Transverse stretch λ_{G2}		
			max	min	avg	max	min	avg	max	min	avg
0	sphere	50	1.32	0.72	0.98	1.44	0.75	1	1.23	0.83	0.97
0	crescent	50	1.5	0.71	0.98	1.3	0.8	1	1.21	0.84	0.98
2	sphere	75	1.36	0.69	0.98	1.26	0.66	1	1.2	0.8	0.98
2	crescent	75	1.31	0.61	0.98	1.24	0.8	1.01	1.34	0.68	0.97
7	sphere	105	1.4	0.79	0.98	1.3	0.57	1	1.2	0.77	0.98
7	crescent	105	1.37	0.59	1	1.6	0.83	1.02	1.16	0.77	0.98
10	sphere	165	1.6	0.73	1.01	1.35	0.6	1.02	1.25	0.75	0.99
10	crescent	165	1.48	0.58	1.01	1.42	0.75	1.02	1.22	0.77	1
15	sphere	225	1.27	0.73	1.01	1.35	0.55	1.02	1.22	0.79	0.98
15	crescent	225	1.34	0.54	1.02	1.37	0.8	1.02	1.32	0.81	1

Table 2: Summary of Acute Deformation. Strains were calculated taking the configuration prior to expansion as the reference and the configuration immediately after the inflation step as the deformed grid. On average, both the sphere and crescent expanders showed similar trends, with values close to 1 which would indicate no deformation. However, due to spatial variations, we measured maximum area changes were as high as 1.60 for the sphere and 1.50 for the crescent. The stretches in the longitudinal and transverse directions were anisotropic, with the maximum values of longitudinal stretches almost always higher than the transverse stretches. (Table adapted with permission from [31])

Discussion

Here we presented a protocol to characterize the deformations induced during a tissue expansion procedure in a porcine model using multi-view stereo (MVS) and isogeometric kinematics (IGA kinematics). During tissue expansion, skin undergoes large deformations going from a smooth and relatively flat surface to a dome-like 3D shape. Skin, like other biological membranes [34], responds to stretch by producing new material, increasing in area that can be then used for reconstructive purposes [35]. Therefore, accurate determination of the stretch produced by an expander is crucial to understand the mechanisms that regulate the adaptation of skin. Planning an expansion procedure is challenging because tissue expanders come in different sizes and shapes, the stretch distribution is not uniform over the entire expanded area and it depends on the location and rate of inflation [11,36]. Having a protocol to accurately estimate expansion-induced deformation and capable of resolving large strains, 3D shapes, and regional variations, opens new avenues to study the mechanical regulation of skin growth, and can eventually lead to quantitative preoperative planning tools. Towards that goal, we developed a non-invasive, affordable, and flexible methodology to measure deformation in a porcine model of skin expansion [32].

Critical Steps

Animal models for tissue expansion have been well characterized for more than two decades [37]. Porcine skin shows comparable properties to human integument. Furthermore, skin expansion in pigs follows a similar procedure as it would be done in humans [38]. The tissue expansion procedure is the cornerstone for the success of this protocol. Experienced surgeons, experts in tissue expansion, performed the technique in the animal model presented here.

Skin is conveniently exposed to the outside environment and it is a thin membrane, therefore its deformation can be characterized by tracking points on its surface [17]. MVS offers a flexible and affordable technique to study 3D skin deformations *in vivo* over long periods of time. This algorithm takes as input a set of photographs from a static scene and uses feature matching across the photographs to extract 3D coordinates. MVS reconstruction and the subsequent kinematic analysis critically depend on the photo acquisition steps of this protocol.

Modifications and Troubleshooting

During tissue expansion, the device can migrate away from the grid due to animal movement and loosening of the pocket in which the expander was originally placed. If the expanded area moves outside of the grid, the expander should be deflated and removed. This problem has been encountered using the protocol in one out of eight grids [31,32]. Expanders can also leak if they are defective or punctured during the inflation protocol. This also compromises the validity of the experiment and the safety of the animal, therefore the expander should be removed. This problem has been encountered using this protocol in one out of eight grids [31,32].

MVS reconstruction can be challenging for some sets of photographs due to lighting effects, lack of focus, and background noise [23]. Even though the commercial tools for MVS are powerful, if the results are not accurate enough at first, the following troubleshooting steps have always corrected the problem in on our experience: manually remove the background in the photographs; select a subset of photographs with sharper focus and discard blurry images; manually select matching points across photographs in the commercial software interface.

Limitations of the Technique

As discussed above, porcine integument is similar to human [38], nevertheless, there are still differences. Therefore, a porcine model is not expected to be fully predictive of human tissue expansion protocols [37]. Another limitation of the protocol is the lack of commercial tools or user-

friendly software to analyze the geometric models. Currently, once the geometry is generated through MVS, the analysis is performed with in-house code which consists of C++ and Python scripts. While on the one hand, the proposed method is creative and offers an affordable, convenient way to study the mechanics of soft tissue over long periods of time, the data analysis is dependent on technologies which have only been popular for the past decade [27]. To circumvent this limitation, we provide our implementation of spline subroutines with this submission. One more limitation is the restriction of a tattooed grid in order to track chronic deformations. The need for a tattooed grid hinders the translation of the protocol to clinical settings.

Significance of the Technique with Respect to Existing/Alternative Methods

Currently, physicians rely mostly on their experience during preoperative planning of tissue expansion procedures, which has led to a wide variety of arbitrary protocols that often differ greatly [13,14,15]. The protocol presented here addresses existing knowledge gaps by quantifying expansion-induced deformation in a porcine animal model of tissue expansion. To the author's knowledge, this is the first protocol to quantify continuous deformation maps on sizable patches of skin tissue [31,32].

The protocol is innovative, non-invasive, affordable and flexible; it relies on recent developments in computer vision algorithms such as MVS, and numerical analysis such as IGA kinematics. MVS has advanced intensely in the past decade, reaching reconstruction errors as low as 2% [24]. The rise in commercially available software as well as open source code showcases the high popularity of this method [41]. MVS is affordable because it requires only a digital camera and photographs are taken without calibration of the camera position. In contrast, other techniques such as stereo reconstruction require additional hardware to control the location of the camera [17]. MVS is flexible because it can be performed in a variety of scenarios as long as photographs can be taken from different angles. This is a feature that becomes more relevant when considering a potential clinical application. In contrast, other techniques such as motion tracking require a specific setup and cannot be performed in an arbitrary location [18]. One more feature of MVS is the production of 3D geometries. Other techniques, such as digital image correlation (DIC), are preferred for 2D motion tracking [39]. The results presented here showcased the ability of commercial algorithms to faithfully reconstruct the 3D shapes induced during tissue expansion.

From the 3D geometries, deformations have to be calculated. This protocol relies on the use of spline surface IGA kinematics. Splines are useful because a few control points parameterize smooth geometries with high continuity which are needed for analysis of thin membranes [40]. The greatest advantage of splines in this application is the notion of a parametric space. Other techniques, such as finite elements, lack a global parameter domain. While this is convenient for certain problems such as simulation of irregular patches (for example patches with holes), having an explicit parameterization allows determination of stretches between any two configurations in a straightforward manner. For instance, two different analyses were shown here: chronic and acute deformations. To calculate the strains in the grids with this protocol it is enough to provide the splines of the two surfaces of interest since all the surfaces have the same parameter domain.

During tissue expansion, skin responds to the applied deformation by growing in surface area, producing new integument that can then be employed for reconstructive surgery. Characterizing clinically relevant deformations of skin over long periods of time can improve our understanding of the mechanobiology of this organ as well as enable the development of quantitative preoperative tools. The protocol described here specifically addresses the need of an experimental design with potential translation to the clinical setting.

Future Applications or Directions after Mastering this Technique

The source code that is used in this protocol could easily be adjusted to other applications and could be incorporated into more user-friendly implementations. Provided with this paper are routines to evaluate spline basis functions, parameterize continuous fields over spline surfaces, integrate those continuous fields, and calculate deformation gradients, membrane and bending strains. We expect that this source code will continue to evolve towards a tool that can be eventually used in real clinical applications of tissue expansion as well as enable other applications. Another future area of work is the refinement of this protocol to take into consideration mechanical properties and stresses in the tissue and not only kinematics.

From a clinically relevant perspective, this protocol is able to quantify regional variations of tissue deformation, as well as differences between different expander shapes and inflation rates [31,32]. Further work is needed to continue to evaluate the effect of different expansion parameters on the tissue response. Moreover, further refinement of the porcine model with emphasis on the biological mechanisms of adaptation can help elucidate fundamental mechanisms regulating skin adaptation to overstretch. The ultimate goal is to validate the protocol in a porcine model in order to translate it to the clinical setting.

Disclosures

SThe authors have nothing to disclose.

Acknowledgements

This work was supported by NIH grant 1R21EB021590-01A1 to Arun Gosain and Ellen Kuhl.

References

1. Gosain, A. K., Zochowski, C. G., & Cortes, W. Refinements of tissue expansion for pediatric forehead reconstruction: a 13-year experience. *Plast Reconstr Surg.* **124**, 1559-1570 (2009).
2. Neumann, C. G. The expansion of an area of skin by progressive distention of a subcutaneous balloon: Use of the Method for Securing Skin for Subtotal Reconstruction of the Ear. *Plast Reconstr Surg.* **19**, 124-130 (1957).

3. De Filippo, R. E., & Atala, A. Stretch and growth: the molecular and physiologic influences of tissue expansion. *Plast Reconstr Surg.* **109**, 2450-2462 (2002).
4. Buganza Tepole, A., Joseph Ploch, C., Wong, J., Gosain, A. K., & Kuhl, E. Growing skin: A computational model for skin expansion in reconstructive surgery. *J Mech Phys Solids.* **59**, 2177-2190 (2011).
5. LoGiudice, J., & Gosain, A. K. Pediatric Tissue Expansion: Indications and Complications. *J Craniofac Surg.* **14**, 866-866 (2003).
6. Rivera, R., LoGiudice, J., & Gosain, A. K. Tissue expansion in pediatric patients. *Clin Plast Surg.* **32**, 35-44 (2005).
7. Marcus, J., Horan, D. B., & Robinson, J. K. Tissue expansion: Past, present, and future. *J Am Acad Dermatol.* **23**, 813-825 (1990).
8. Patel, P. A., Elhadi, H. M., Kitzmiller, W. J., Billmire, D. A., & Yakuboff, K. P. Tissue expander complications in the pediatric burn patient: a 10-year follow-up. *Ann Plast Surg.* **72**, 150-154 (2014).
9. Pietramaggiori, G. *et al.* Tensile Forces Stimulate Vascular Remodeling and Epidermal Cell Proliferation in Living Skin. *Ann Surg.* **246**, 896-902 (2007).
10. Khalatbari, B., & Bakhshaeekia, A. Ten-year experience in face and neck unit reconstruction using tissue expanders. *Burns.* **39**, 522-527 (2013).
11. Brobmann, F. F., & Huber, J. Effects of different-shaped tissue expanders on transluminal pressure, oxygen tension, histopathologic changes, and skin expansion in pigs. *Plast Reconstr Surg.* **76**, 731-736 (1985).
12. Rappard, J. H., Molenaar, J., van Doorn, K., Sonneveld, G. J., & Borghouts, J. M. Surface-area increase in tissue expansion. *Plast Reconstr Surg.* **82**, 833-839 (1988).
13. Pusic, A. L., & Cordeiro, P. G. An accelerated approach to tissue expansion for breast reconstruction: experience with intraoperative and rapid postoperative expansion in 370 reconstructions. *Plast Reconstr Surg.* **111**, 1871-1875 (2003).
14. Schneider, M. S., Wyatt, D. B., Konvolinka, C. W., Hassanein, K. M., & Hiebert, J. M. Comparison of Rapid Versus Slow Tissue Expansion on Skin-Flap Viability. *Plast Reconstr Surg.* **92**, 1126-1132 (1993).
15. Schmidt, S. C., Logan, S. E., Hayden, J. M., Ahn, S. T., & Mustoe, T. A. Continuous versus conventional tissue expansion: experimental verification of a new technique. *Plast Reconstr Surg.* **87**, 10-15 (1991).
16. Buganza Tepole, A., Gart, M., Purnell, C. A., Gosain, A. K., & Kuhl, E. Multi-view stereo analysis reveals anisotropy of prestrain, deformation, and growth in living skin. *Biomech Model Mechanobiol.* **14**, 1007-1019 (2015).
17. Tonge, T. K., Atlan, L. S., Voo, L. M., & Nguyen, T. D. Full-field bulge test for planar anisotropic tissues: Part I-Experimental methods applied to human skin tissue. *Acta Biomater.* **9**, 5913-5925 (2013).
18. Park, S. I., & Hodgins, J. K. Capturing and animating skin deformation in human motion. *ACM Trans Graph.* **25,** 881-881 (2006).
19. Rausch, M. K. *et al.* In vivo dynamic strains of the ovine anterior mitral valve leaflet. *J Biomech.* **44**, 1149-1157 (2011).
20. Leyva-Mendivil, M. F., Page, A., Bressloff, N. W., & Limbert, G. A mechanistic insight into the mechanical role of the stratum corneum during stretching and compression of the skin. *J Mech Behav Biomed Mater.* **49**, 197-219 (2015).
21. Buganza Tepole, A., Kabaria, H., Bletzinger, K.-U., & Kuhl, E. Isogeometric Kirchhoff-Love shell formulations for biological membranes. *Comput Methods Appl Mech Eng.* **293**, 328-347 (2015).
22. Prot, V., Skallerud, B., & Holzapfel, G. A. Transversely isotropic membrane shells with application to mitral valve mechanics. Constitutive modelling and finite element implementation. *Int J Num Meth Eng.* **71**, 987-1008, 10.1002/nme.1983 (2007).
23. Seitz, S. M., Curless, B., Diebel, J., Scharstein, D., & Szeliski, R. A comparison and evaluation of multi-view stereo reconstruction algorithms. *Proc IEEE CVPR.* **1**, 519-528, 10.1109/CVPR.2006.19 (2006).
24. Furukawa, Y., & Ponce, J. Dense 3D motion capture for human faces. *2009 IEEE CVPR.* (2009).
25. Jor, J. W. Y., Nash, M. P., Nielsen, P. M. F., & Hunter, P. J. Estimating material parameters of a structurally based constitutive relation for skin mechanics. *Biomech Model Mechanobiol.* **10**, 767-778 (2010).
26. Weickenmeier, J., Jabareen, M., & Mazza, E. Suction based mechanical characterization of superficial facial soft tissues. *J Biomech.* **48**, 4279-4286 (2015).
27. Hughes, T. J. R., Cottrell, J. A., & Bazilevs, Y. Isogeometric analysis: CAD, finite elements, NURBS, exact geometry and mesh refinement. *Comput Methods Appl Mech Eng.* **194** 4135-4195 (2005).
28. Echter, R., Oesterle, B., & Bischoff, M. A hierarchic family of isogeometric shell finite elements. *Comput Methods Appl Mech Eng.* **254**, 170-180 (2013).
29. Benson, D. J., Hartmann, S., Bazilevs, Y., Hsu, M. C., & Hughes, T. J. R. Blended isogeometric shells. *Comput Methods Appl Mech Eng.* **255**, 133-146 (2013).
30. Chen, L. *et al.* Explicit finite deformation analysis of isogeometric membranes. *Comput Methods Appl Mech Eng.* **277**, 104-130 (2014).
31. Buganza Tepole, A., Gart, M., Purnell, C. A., Gosain, A. K., & Kuhl, E. The Incompatibility of Living Systems: Characterizing Growth-Induced Incompatibilities in Expanded Skin. *Ann Biomed Eng.* **44**, 1734-1752 (2016).
32. Buganza Tepole, A., Gart, M., Gosain, A. K., & Kuhl, E. Characterization of living skin using multi-view stereo and isogeometric analysis. *Acta Biomater.* **10**, 4822-4831 (2014).
33. Rose, E. H., Ksander, G. A., & Vistnes, L. M. Skin tension lines in the domestic pig. *Plast Reconstr Surg.* **57**, 729-732 (1976).
34. Rausch, M. K., & Kuhl, E. On the mechanics of growing thin biological membranes. *J Mech Phys Solids.* **63**, 128-140 (2014).
35. Argenta, L. C. Controlled tissue expansion in reconstructive surgery. *Br J Plast Surg.* **37**, 520-529 (1984).
36. Hudson, D. Maximising the use of tissue expanded flaps. *Br J Plast Surg.* **56**, 784-790 (2003).
37. Bartell, T. H., & Mustoe, T. A. Animal models of human tissue expansion. *Plast Reconstr Surg.* **83**, 681-686 (1989).
38. Belkoff, S. M. *et al.* Effects of subcutaneous expansion on the mechanical properties of porcine skin. *J Surg Res.* **58**, 117-123 (1995).
39. Annaidh, A., Bruyère, K., Destrade, M., Gilchrist, M. D., & Otténio. Automated estimation of collagen fibre dispersion in the dermis and its contribution to the anisotropic behaviour of skin. *Ann Biomed Eng.* **5**, 139-148 (2012).
40. Kiendl, J., Bletzinger, K. U., Linhard, J., & Wüchner, R. Isogeometric shell analysis with Kirchhoff-Love elements. *Comput Methods Appl Mech Eng.* **198**, 3902-3914 (2009).
41. Changchang, W. VisualSFM: *A Visual Structure from Motion System.* http://ccwu.me/vsfm/index.html (2011).

